Multiple-array passive acoustic source localization in shallow water

Dag TollefsenPeter Gerstoft and William S. Hodgkiss

Citation: The Journal of the Acoustical Society of America **141**, 1501 (2017); doi: 10.1121/1.4976214
View online: http://dx.doi.org/10.1121/1.4976214
View Table of Contents: http://asa.scitation.org/toc/jas/141/3
Published by the Acoustical Society of America

Multiple-array passive acoustic source localization in shallow water

Dag Tollefsen[a)]
Norwegian Defence Research Establishment (FFI), Box 115, 3191 Horten, Norway

Peter Gerstoft and William S. Hodgkiss
Scripps Institution of Oceanography, University of California San Diego, La Jolla, California 92093, USA

(Received 7 May 2016; revised 16 January 2017; accepted 30 January 2017; published online 6 March 2017)

This paper considers concurrent matched-field processing of data from multiple, spatially-separated acoustic arrays with application to towed-source data received on two bottom-moored horizontal line arrays from the SWellEx-96 shallow water experiment. Matched-field processors are derived for multiple arrays and multiple-snapshot data using maximum-likelihood estimates for unknown complex-valued source strengths and unknown error variances. Starting from a coherent processor where phase and amplitude is known between all arrays, likelihood expressions are derived for various assumptions on relative source spectral information (amplitude and phase at different frequencies) between arrays and from snapshot to snapshot. Processing the two arrays with a coherent-array processor (with inter-array amplitude and phase known) or with an incoherent-array processor (no inter-array spectral information) both yield improvements in localization over processing the arrays individually. The best results with this data set were obtained with a processor that exploits relative amplitude information but not relative phase between arrays. The localization performance improvement is retained when the multiple-array processors are applied to short arrays that individually yield poor performance. © *2017 Acoustical Society of America*.
[http://dx.doi.org/10.1121/1.4976214]

[ZHM] Pages: 1501–1513

I. INTRODUCTION

Matched-field processing (MFP) is a well-established technique for source localization with a single array, suitable for application in shallow water where multipath propagation can yield information to infer the source range and depth.[1–14] MFP is based on matching the acoustic pressure field on a hydrophone array with modeled replica fields computed for the acoustic waveguide via a numerical propagation model over a grid of possible source positions, with the position estimate typically taken to be the grid point of the best match. In MFP, the localization performance of single acoustic arrays has been studied extensively,[15,16] but there appears to have been little work on MFP applied to the simultaneous processing of data from multiple, spatially-separated arrays. Zurk *et al.*[10] applied adaptive MFP to data from three vertical line arrays (VLAs) in shallow water (the SBCX experiment), and used pre-computed inter-array phase and amplitude differences based on non-acoustic source motion information and known array geometries to achieve a coherent-array processing gain. Nicholas *et al.*[11] applied MFP to an array with co-located vertical and horizontal apertures (an L-shaped array) and considered coherent processing of all array elements as well as incoherent combination of processors applied to the two legs of the array, and found that the two approaches performed nearly equal. Coherent processing of distributed sensors has more recently been considered in other contexts,[17] but is there applied to plane-wave Bartlett beamforming. Data from multiple separated acoustic arrays have been collected and considered in applications to marine mammal localization;[18] however, most of these applications consider source location estimates from each array processed individually, then combined in a subsequent tracking step, and do not combine acoustic data between sensor systems. MFP with multiple arrays has recently been studied with simulated data for a network of acoustic arrays in an urban multipath environment,[19] and for simulated data for shallow-water scenarios with multiple horizontal and vertical arrays.[20] Both studies observed that while spatially coherent processing of multiple arrays can yield significant improvement in localization performance over incoherent processing (of multiple arrays), it can also be more susceptible to model mismatch (than incoherent processing). An alternative multiple-array matched-field processor was recently proposed and found to be more robust to model mismatch (than a coherent processor) in some scenarios.[20] Potential limitations to application of MFP to data from spatially-separated arrays include inter-array mismatch,[19,20] environmental mismatch,[21–24] signal coherence/array length considerations for horizontal line arrays (HLAs),[15] and effects of random spatial/temporal fluctuations in the ocean on signal coherence.[25]

This paper considers MFP for source localization with spatially-separated acoustic arrays in shallow water. Specifically, we consider concurrent MFP of data from two HLAs deployed on the seafloor in the SWellEx-96 data set.[5,7–9] Matched-field processors are developed for multiple

a)Electronic mail: dag.tollefsen@ffi.no

arrays using maximum-likelihood (ML) expressions for unknown complex source strengths and unknown error variance for various assumptions on relative source spectral information (amplitude and phase) between arrays (Sec. II). The processors are applied to simulated HLA data in a shallow water scenario, and effects of inter-array phase and inter-array amplitude errors on source localization performance are examined (Sec. III). The processors are then applied to towed-source data received on two HLAs from Event S5 of the SWellEx-96 data set (Sec. IV). A summary and discussion is presented in Sec. V.

II. THEORY

The data consist of complex acoustic fields measured at F frequencies and J sensor arrays, each with N_j sensor, with time segmented into K subsegments (snapshots), i.e., $\mathbf{d} = \{\mathbf{d}_{fjk}, f=1,F;\ j=1,J;\ k=1,K\}$. The source–receiver range is assumed constant over the K snapshots. The source spectrum (amplitude and phase) is considered unknown over frequency. The data errors are assumed complex, circularly symmetric Gaussian-distributed random variables, with zero mean and unknown variances which depend on frequency but are considered constant across arrays and over the K snapshots. In this case, the likelihood function is given by

$$L(\mathbf{x}) = \prod_{f=1}^{F}\prod_{k=1}^{K}\frac{1}{\pi^N|\mathbf{\Sigma}_f|}\exp\Big[\big(\mathbf{d}_{fk} - S_{fk}\mathbf{d}_f(\mathbf{x})\big)^H \times\mathbf{\Sigma}_f^{-1}\big(\mathbf{d}_{fk} - S_{fk}\mathbf{d}_f(\mathbf{x})\big)\Big], \tag{1}$$

where we have defined data and replica vectors concatenated over J arrays

$$\mathbf{d}_{fk} = \Big[\mathbf{d}_{f1k}^T, \ldots, \mathbf{d}_{fJk}^T\Big]^T, \tag{2}$$
$$\mathbf{d}_f(x) = \Big[\mathbf{d}_{f1}^T(x), \ldots, \mathbf{d}_{fJ}^T(x)\Big]^T,$$

with T the matrix transpose. Each vector is of size $N = \sum_{j=1}^{J} N_j$, and $\mathbf{d}_f(\mathbf{x})$ are the replica acoustic fields due to a unit-amplitude, zero-phase source at frequency f and location $\mathbf{x}$, and $S_{fk} = A_{fk}e^{i\theta_{fk}}$ are the unknown complex source strength (amplitude and phase) terms (considered below). In the following, we assume a diagonal error covariance matrix $\mathbf{\Sigma}_f$ with the same error variances ν_f on hydrophones across all arrays:

$$\mathbf{\Sigma}_f = \nu_f\mathbf{I}_N. \tag{3}$$

If the relative array calibrations or array time-synchronizations are poorly known, we assume a source term S_{fjk} for each array (index j). This gives

$$L(\mathbf{x},\nu_f) = \prod_{f=1}^{F}\frac{1}{(\pi\nu_f)^{NK}} \times\exp\left\{-\sum_{j=1}^{J}\sum_{k=1}^{K}\|\mathbf{d}_{fjk} - S_{fjk}\mathbf{d}_{fj}(\mathbf{x})\|^2/\nu_f\right\} = \prod_{f=1}^{F}\frac{1}{(\pi\nu_f)^{NK}}\exp\left\{-\frac{\phi_f}{\nu_f}\right\}, \tag{4}$$

with

$$\phi_f(\mathbf{x}) = \sum_{j=1}^{J}\sum_{k=1}^{K}\|\mathbf{d}_{fjk} - S_{fjk}\mathbf{d}_{fj}(\mathbf{x})\|^2, \tag{5}$$

where for perfect arrays the source term is independent of array index j. We also assume that the number of snapshots K is equal at all arrays. The unknown error variances ν_f represent data errors (measurement noise) and model errors for each hydrophone.

A. Error variance

For unknown error variances, we apply ML-estimates.[26–28] Differentiating L, Eq. (4) with respect to ν_f and setting it equal to zero yields the ML-estimate for the variances

$$\hat{\nu}_f(\mathbf{x}) = \frac{1}{KN}\phi_f(\mathbf{x}). \tag{6}$$

Substituting the estimate from Eq. (6) for the variance into Eq. (4), we obtain the likelihood function

$$L(\mathbf{x}) = \prod_{f=1}^{F}\left(\frac{\pi\phi_f(\mathbf{x})}{KN}\right)^{-KN}\exp\{-KN\} = (e\pi)^{-FKN}\exp\left\{-KN\sum_{f=1}^{F}\log_e\big(\phi_f(\mathbf{x})/KN\big)\right\} = (e\pi)^{-FKN}\exp\big\{-E(\mathbf{x})\big\}, \tag{7}$$

with the corresponding negative log-likelihood (error) function

$$E(\mathbf{x}) = KN\sum_{f=1}^{F}\log_e(\phi_f(\mathbf{x})/K) - FKN\log_e N. \tag{8}$$

The constant term $-FKN\log_e N$ is omitted in the following.

B. Source term

So far, the general form of the complex source terms S_{fjk} has been retained. Next, we employ ML-solutions for unknown source amplitude and phase. ML processors can be derived under varying assumptions on relative source spectral information (amplitude and phase) between snapshots and frequencies.[26,29] For multiple arrays, ML processors can be derived under varying assumptions also on relative source spectral information between arrays.[20] Three cases of inter-array spectral information are considered:

(1) Coherent: Relative amplitude and relative phase known between arrays (i.e., relative array calibrations known and arrays synchronized in time;
(2) Incoherent: Unknown amplitude and unknown phase between arrays (i.e., relative array calibration not known and arrays not synchronized in time; and
(3) Relative Amplitude: Relative amplitude known but unknown phase between arrays (i.e., relative array calibrations known but arrays not synchronized in time.

Furthermore, we assume the source amplitude is constant across snapshots (i.e., is constant over the K snapshots), while the source phase is unknown (i.e., not predictable) from snapshot to snapshot.[29] This model would fit well to narrowband source tows or ship tonals. For broadband data (e.g., ship broadband radiated noise) the amplitude is also likely to vary across snapshots. We assume no relative knowledge of source amplitude or phase from frequency to frequency.

The assumptions and the appropriate source terms are summarized in Table I, where processors assuming also varying amplitude across snapshots are included (see the Appendix).

1. Coherent

This case corresponds to the ideal case of one big array. The relative amplitude and the relative phase spectra are both known between arrays (i.e., relative array calibrations are known and all arrays are synchronized in time). The source term is then $S_{fk} = A_f e^{i\theta_{fk}}$(i.e., no dependence on array index j and only phase varies across snapshots). Maximizing the likelihood by setting $\partial E/\partial A_f = 0$ and $\partial E/\partial\theta_{fk} = 0$ leads to the ML amplitude and phase estimates

$$A_f = \frac{\sum_{k=1}^{K} |\mathbf{d}_f^H(\mathbf{x})\mathbf{d}_{fk}|}{K\|\mathbf{d}_f(\mathbf{x})\|_2^2}, \quad e^{i\theta_{fk}} = \left[\frac{\mathbf{d}_f^{\mathrm{H}}(\mathbf{x})\mathbf{d}_{fk}}{\mathbf{d}_{fk}^{\mathrm{H}}\mathbf{d}_f(\mathbf{x})}\right]^{1/2}. \tag{9}$$

Substituting these expressions into Eqs. (5) and (8) leads to the ML processor for relative amplitude and phase information known between arrays, termed the *coherent array processor* and denoted E_{COH}:

$$E_{\mathrm{COH}} = KN\sum_{f=1}^{F}\log_e\left\{\mathrm{Tr}\{\mathbf{C}_f\} - \frac{\left(\sum_{k=1}^{K}|\mathbf{d}_{fk}^{\mathrm{H}}\mathbf{d}_f(\mathbf{x})|\right)^2}{K^2\|\mathbf{d}_f(\mathbf{x})\|_2^2}\right\}, \tag{10}$$

where we have defined the data sample covariance matrix (SCM)

$$\mathbf{C}_f = \frac{1}{K}\sum_{k=1}^{K}\mathbf{d}_{fk}^{\mathrm{H}}\mathbf{d}_{fk}, \tag{11}$$

with trace $\mathrm{Tr}\{\mathbf{C}_f\} = K^{-1}\sum_{k=1}^{K}\|\mathbf{d}_{fk}\|_2^2$.

TABLE I. ML multiple-array processors and source terms for various states of knowledge of relative amplitude and phase between arrays and snapshots. See text for symbol definitions [r—relative knowledge, u—unknown].

Amplitude array/snapshot	Phase array/snapshot	Source term	ML-processor	Equation
r/r	r/u	$A_f e^{i\theta_{fk}}$	E_{COH}	(10)
r/u	r/u	$A_{fk} e^{i\theta_{fk}}$	E_{COH}^{uu}	(A2)
u/r	u/u	$A_{fj} e^{i\theta_{fjk}}$	E_{INC}	(13)
u/u	u/u	$A_{fjk} e^{i\theta_{fjk}}$	E_{INC}^{uu}	(A4)
r/r	u/u	$A_f e^{i\theta_{fjk}}$	E_{RelAmp}	(15)
r/u	u/u	$A_{fk} e^{i\theta_{fjk}}$	E_{RelAmp}^{uu}	(A7)

2. Incoherent

With no spectral information available between arrays, the source term is $S_{fjk} = A_{fj} e^{i\theta_{fjk}}$ (amplitude A_{fj} unknown over both frequency and array, and phase θ_{fjk} unknown over frequency, array, and snapshot). Maximizing the likelihood by setting $\partial E/\partial A_{fj} = 0$ and $\partial E/\partial\theta_{fjk} = 0$ leads to the ML amplitude and phase estimates

$$A_{fj} = \frac{\sum_{k=1}^{K} |\mathbf{d}_{fj}^H(\mathbf{x})\mathbf{d}_{fjk}|}{K\|\mathbf{d}_{fj}(\mathbf{x})\|_2^2}, \quad e^{i\theta_{fjk}} = \left[\frac{\mathbf{d}_{fj}^{\mathrm{H}}(\mathbf{x})\mathbf{d}_{fjk}}{\mathbf{d}_{fjk}^{\mathrm{H}}\mathbf{d}_{fj}(\mathbf{x})}\right]^{1/2}. \tag{12}$$

Substituting these expressions into Eqs. (5) and (8) leads to the ML processor for unknown inter-array amplitude and phase, termed the *incoherent-array processor* and denoted E_{INC}

$$E_{\mathrm{INC}} = KN\sum_{f=1}^{F}\log_e\left\{\mathrm{Tr}\{\mathbf{C}_f\} - \sum_{j=1}^{J}\frac{\left(\sum_{k=1}^{K}|\mathbf{d}_{fjk}^{\mathrm{H}}\mathbf{d}_{fj}(\mathbf{x})|\right)^2}{K^2\|\mathbf{d}_{fj}(\mathbf{x})\|_2^2}\right\}. \tag{13}$$

This processor can also be applied to arrays individually. Note that the frequency-incoherent Bartlett processor often applied to single arrays makes the additional assumption of relative amplitude unknown across snapshots (i.e., both relative amplitude and phase unknown across snapshots), see Eq. (A4).

3. Relative amplitude

Third, we consider an intermediate case where relative amplitudes (amplitude ratios) are known for all arrays (i.e., relative array calibrations known) but relative phase is unknown between arrays (i.e., arrays are not synchronized with each other in time).[20] The source term is $S_{fjk} = A_f e^{i\theta_{fjk}}$(i.e., amplitude depends only on frequency while phase depends on frequency, array, and snapshot). Maximizing the likelihood by setting $\partial E/\partial A_f = 0$ and $\partial E/\partial\theta_{fjk} = 0$ gives

$$A_f = \frac{\sum_{k=1}^{K}\sum_{j=1}^{J} |\mathbf{d}_{fj}^{\mathrm{H}}(\mathbf{x})\mathbf{d}_{fjk}|}{K\|\mathbf{d}_f(\mathbf{x})\|_2^2}, \quad e^{i\theta_{fjk}} = \left[\frac{\mathbf{d}_{fj}^{\mathrm{H}}(\mathbf{x})\mathbf{d}_{fjk}}{\mathbf{d}_{fjk}^{\mathrm{H}}\mathbf{d}_{fj}(\mathbf{x})}\right]^{1/2}. \tag{14}$$

Substituting these expressions into Eqs. (5) and (8) leads to the ML processor for relative amplitude known and relative phase unknown between arrays, termed the *relative-amplitude array processor* and denoted E_{RelAmp}

$$E_{\mathrm{RelAmp}} = KN\sum_{f=1}^{F}\log_e\left\{\mathrm{Tr}\{\mathbf{C}_f\} - \frac{\left(\sum_{k=1}^{K}\sum_{j=1}^{J}|\mathbf{d}_{fjk}^{\mathrm{H}}\mathbf{d}_{fj}(\mathbf{x})|\right)^2}{K^2\|\mathbf{d}_f(\mathbf{x})\|_2^2}\right\}. \tag{15}$$

This processor assumes known relative amplitude calibration between arrays but does not assume time-synchronization between arrays.

III. SIMULATION STUDY

In this section, the localization performance of the multiple-array processors [E_{COH} Eq. (10), E_{INC} Eq. (13), and E_{RelAmp} Eq. (15)] is studied with one and two HLAs in a simulated shallow-water scenario similar to the SWellEx-96 experiment discussed in detail in Sec. III A.

A. Localization with HLAs

The test case involves a shallow water environment of water depth 100 m, a semi-infinite seabed with sound speed 1580 m/s, density 1.50 g/cm^3, and attenuation 0.16 dB/m-kHz. The sound-speed in water decreases from 1514 m/s at 0 m to 1510 m/s at 100 m depth. A 10 km by 10 km area is considered. A HLA of length 256 m with 48 equidistantly spaced hydrophones is placed at the seabed, centered at (east, north) position (6.0, 7.0) km, and oriented east–west. A second array position (7.5, 3.5) km, 3.8 km from the first position, also is considered. The two positions are henceforth labelled N and S. A source at depth 20 m and position (2.0, 5.5) km transmits a signal at three frequencies of 200, 300, and 400 Hz. The array signal-to-noise ratio (SNR), defined by $\mathrm{SNR} = 10\log_{10}(\|\mathbf{d}_{fj}\|_2^2/\|\mathbf{n}_{fj}\|_2^2)$ with $\mathbf{d}_{fj}$ the noise-free data vector and $\mathbf{n}_{fj}$ the complex noise vector over the array at fth frequency and jth position, is set to −6 dB at all frequencies (N position). With the same source strength and noise variances, the SNRs in the S position are then −4.8, −6.2, and −5.5 dB, respectively, at the three frequencies, due to propagation effects. The synthetic data and replica fields were computed with the acoustic propagation model ORCA with the complex-valued mode search.[34] The three-dimensional (3D) replica volume covers 0–10 km in the two horizontal directions (100 m spacing), and 4–98 m in depth (2 m spacing).

Figure 1 (upper row) shows two-dimensional (2D) slices of the 3D ambiguity volumes, from processing [using E_{INC}, Eq. (13), with $J = 1$] of data from the 256-m long HLA in positions N (left column) and in S (second column). The slices are taken at the depth of the minimum of the ambiguity volumes, the depth indicated in lower left corner of each panel. The 3D-position estimate is defined by this minimum value. The color scale for each panel corresponds to the processor values relative to the minimum-misfit value, with bright colors corresponding to low processor values (low misfit). Note that the processor comprises a logarithm of misfits and thus is not expressed in dB. The true (crossing point of the dashed lines) and estimated (circle) source position is indicated on each panel. In both array positions, the array localizes the source in position and depth. Due to the inherent left/right ambiguity of a HLA there is an ambiguous source position estimate in the mirror direction about the array length axis.

Next, consider localization with short HLAs, each of length 128 m and with 24 equidistantly spaced hydrophones (half of the array considered above). The array SNR is set to −9 dB in the N position (−9.2, −8.4, and −4.2 dB, respectively, at the three frequencies, in the S position). Figure 1 (middle row) shows 2D slices of the 3D ambiguity volumes, from localization with the 128-m array in the N position (first column) and in the S position (second column). In either position, the HLA does not localize the source. Processing of two 128-m HLAs (in positions N and S) with multiple-array processors may, however, yield correct localization. Figure 1 (middle row) shows 2D slices of the 3D ambiguity volumes from processing the two HLAs with the coherent multiple-array processor E_{COH} [Eq. (10)] (third

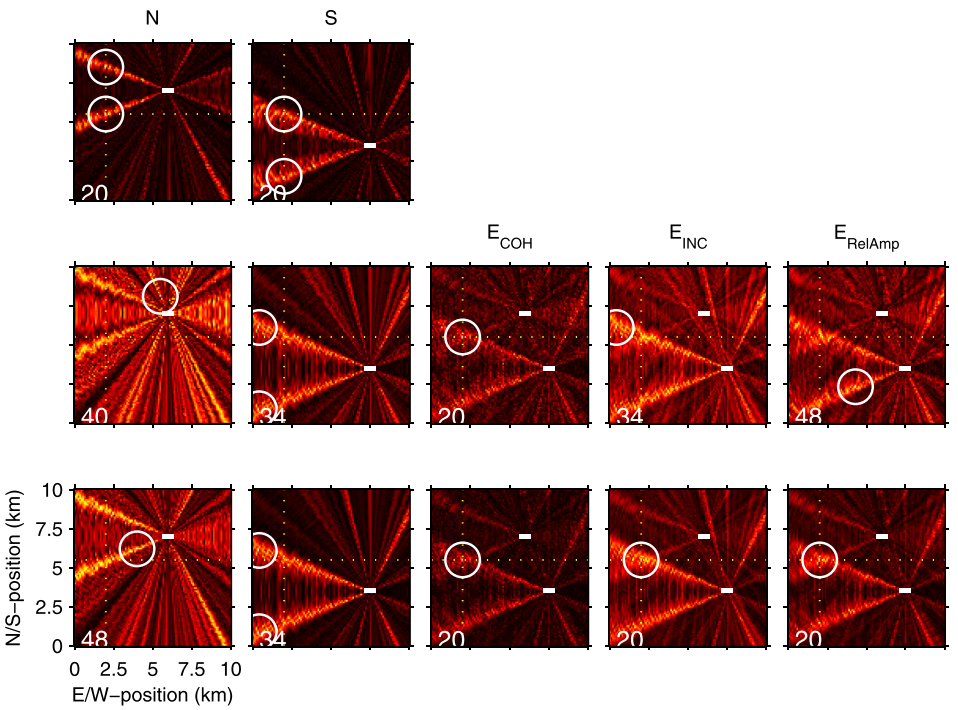

FIG. 1. (Color online) Horizontal slices of 3D-ambiguity volumes for simulated data with HLAs (in N and S positions) processed separately (left columns), and two HLAs processed with multiple-array processors E_{COH} (third column), E_{INC} (fourth column), and E_{RelAmp} (right column). With 256-m length arrays (upper row) at −6 dB SNR, 128-m length arrays at −9 dB SNR (middle row), and 128-m arrays at −6 dB SNR (bottom row). The white circle is centered at the position estimate, the true source position is at the crossing of the dashed white lines, and the white lines indicate arrays. The number (lower left) is the depth estimate and slice depth, the true source depth is 20 m.

column), the incoherent multiple-array processor E_{INC} [Eq. (13)] (fourth column), and the relative amplitude multiple-array processor E_{RelAmp} [Eq. (15)] (fifth column). The color scale for each panel corresponds to the processor values relative to the minimum-misfit value for each processor, with bright colors corresponding to low processor values (low misfit). Note that all processors [Eqs. (10), (13), and (15)] comprise logarithms of misfits and thus are not expressed in dB. For this example, the coherent multiple-array processor E_{COH} correctly localizes the source in position and depth, while the other two multiple-array processors do not. Finally, consider increasing the SNR by 3 dB to −6 dB at the N array (−6.2, −5.4, and −1.2 dB, respectively, at the three frequencies, at the S array). Figure 1 (lower row) shows results from processing the 128-m arrays individually and with the multiple-array processors. With all three multiple-array processors, the source now is correctly localized in position and depth which is not the case when the arrays are processed individually.

B. Localization performance

The examples in Sec. III A illustrate that joint processing of spatially-separated arrays may improve localization relative to individual arrays. Based on the examples, the optimal choice of processor appears to be the coherent-array processor E_{COH} (since this processor uses more information). However, the other two processors may also yield correct localization, dependent on SNR. In this section, we evaluate the relative performance of the three multiple-array processors for different SNRs, and for other source positions than the single case considered above. To evaluate localization performance, we apply Monte Carlo analysis to the test case (with 128-m HLAs in positions N and S, data at three frequencies of 200, 300, and 400 Hz). Here, 400 realizations of random source positions are generated, with a random noise vector added to achieve a given array SNR (specified at the N array). The root-mean-square (RMS) range and depth errors of the source location estimates are computed and used to evaluate localization performance. The fraction of correct localizations (FCL) is also evaluated, defined as the number of localizations within an acceptable range and depth of the true source positions (here set to 0.2 km in range and ±4 m in depth) divided by the total number of realizations.

Figure 2 (left panels) shows the RMS range and depth errors with the three multiple-array processors for SNR varying from −15 to 0 dB (in steps of 3 dB). The RMS range error with all processors decreases from about 3 km at −15 dB to less than 0.2 km at 0 dB SNR. For SNRs from −6 to 0 dB, the range error is lowest with E_{COH}, and lower with E_{RelAmp} than with E_{INC}. For example, at −6 dB SNR, the RMS range error is 1.05, 1.16, and 1.27 km, respectively, with the three processors. The RMS depth error with all processors decreases from above 20 m at −15 dB to less than 13 m at 0 dB SNR. For SNRs from −6 to 0 dB, the depth error is lowest with E_{COH}, and lower with E_{RelAmp} than with E_{INC}. For example, at −6 dB SNR, the RMS depth error is 16.6, 20.6, and 22.8 m, respectively, with the three

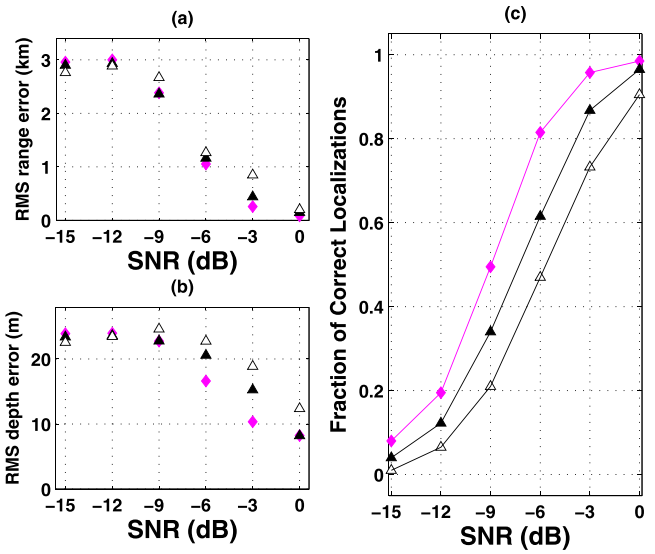

FIG. 2. (Color online) (a) RMS range error, (b) RMS depth error, and (c) FCL versus SNR from processing two 128-m HLAs with the multiple-array processors E_{COH} (diamonds), E_{INC} (open triangles), and E_{RelAmp} (triangles).

processors. This demonstrates that overall, the range and depth localization errors with multiple-array processors reduce with added inter-array amplitude and phase information applied in the processors. The relatively poor depth localization performance can be attributed to the short length of the HLAs (on the order of the water depth). Depth resolution with HLAs is related to the array effective vertical aperture,[15] which diminishes with array length and diminishes from array endfire to broadside directions.

Figure 2(c) shows the FCL at SNRs from −15 to 0 dB, for the multiple-array processors E_{COH} (diamonds), E_{INC} (open triangles), and E_{RelAmp} (triangles). The FCL increases from 0.01–0.08 at −15 dB to 0.90–0.99 at 0 dB SNR. For all SNRs, the performance with E_{RelAmp} better than with E_{INC}, with overall best performance with E_{COH}. For example, at −6 dB the FCL increases from 0.47 with E_{INC} to 0.61 with E_{RelAmp} (an increase of 30%) and to 0.82 with E_{COH} (an increase of 74% over E_{INC} and 34% over E_{RelAmp}). The increase in performance with added inter-array amplitude and phase information is significant at all SNRs.

C. Effects of relative phase and amplitude error

With multiple-array processors that apply inter-array amplitude and phase information, array/system mismatch may degrade localization performance.[19,20] The coherent-array processor E_{COH} assumes phase coherence between arrays, while the other two processors do not. For situations where this assumption may not hold, it is of interest to examine the effects of relative (inter-array) phase error on localization performance. Similarly, E_{COH} and the relative-amplitude processor E_{RelAmp} assume relative amplitude known between arrays, and it is of interest to examine the effects of relative (inter-array) amplitude error on localization performance.

To study effects of relative phase error, a phase factor $\xi = e^{i\beta}$ is applied to the pressure vector of the S array. This simulates degraded phase coherence between the arrays,

while phase coherence within each array is not affected. Phase error can be due to system effects, e.g., a constant relative error in time synchronization between arrays. In this case modeled as a constant but frequency-dependent phase shift $\beta = 2\pi f \Delta t$ for time synchronization error Δt. Phase error can also be due to propagation effects, e.g., temporal fluctuations differing between source to array propagation paths. In this case modeled as a random phase shift with β a random number drawn from a uniform distribution $[0,2\pi]$. Amplitude error can be due to system effects, e.g., a constant (but unknown) relative array calibration offset. To study effects of relative amplitude error, the replica field magnitude on the S array is reduced by a constant factor.

Figure 3 shows the RMS range and depth errors and the FCL with the three multiple-array processors in the presence of: no error (0), time synchronization error of 0.1 ms (T1), relative amplitude error of 2 dB (A2) and 4 dB (A4), time synchronization error of 0.5 ms (T5), and random relative phase error (RP). The test example is with two 128-m length HLAs (in positions N and S), and three processing frequencies (200, 300, and 400 Hz) at −6 dB SNR (at the N array). The multiple-array processors affected by relative errors are E_{RelAmp} (triangles), and E_{COH} (diamonds). For comparison, results with E_{INC} (open triangles), which is unaffected by relative phase and relative amplitude errors, is also plotted. Cases T1 and A2 both represent relatively small errors, and do not alter the relative performance of the processors. With large relative amplitude error (A4) the RMS range error with E_{RelAmp} increases [from 1.16 km (no error) to 1.6 km (A4)] and the FCL with E_{RelAmp} decreases, from 0.62 (no error) to 0.38 (A4), such that this processor yields overall poorest performance. Processor E_{COH} also is degraded by large relative amplitude error, but the FCL with E_{COH} is still much higher than with E_{INC} (and with E_{RelAmp}). With large time synchronization error (T5) the performance with E_{COH} is degraded, from 0.82 (no error) to 0.48 (A4), and processor E_{RelAmp} yields the best performance. With random relative phase error, the FCL with E_{COH} is significantly degraded, from 0.82 (no error) to 0.26 (RP), such that the performance with this processor is much lower than with E_{INC} and with E_{RelAmp}, and in fact yields poorest performance of all cases considered.

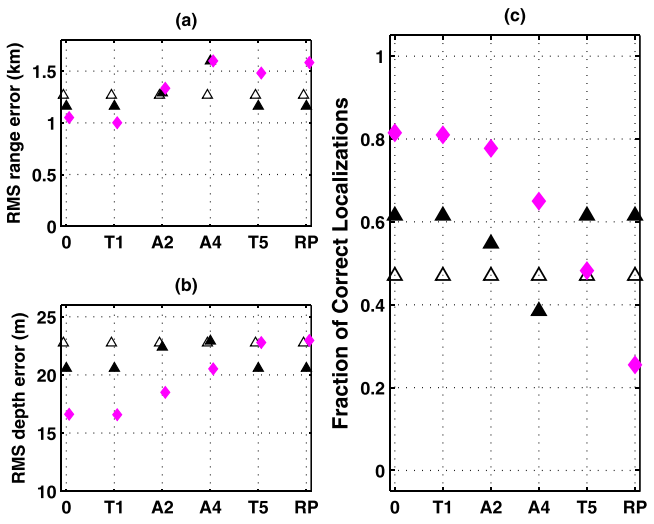

FIG. 3. (Color online) (a) RMS range error, (b) RMS depth error, and (c) FCL at SNR −6 dB from processing two 128-m HLAs with multiple-array processors with no error (0), relative (inter-array) time synchronization error (T1,T5), relative amplitude error (A2,A4), and random relative phase error (RP). The processors are E_{COH} (diamonds), E_{INC} (open triangles), and E_{RelAmp} (triangles).

Other sources of error can also contribute to degraded localization performance. Environmental mismatch is a well-studied problem in matched-field localization.[21–24] With multiple arrays, error in relative array positions and error due to finite replica grid discretization can cause relative phase errors similar to time synchronization error. It is difficult to assess which of the error cases examined is most realistic. Arrays used in MFP must be calibrated, and relative array calibration information is typically available. For time-synchronized arrays, the study here indicates that synchronization (with E_{COH}) should be highly accurate (to within fractions of a millisecond for the case studied). Overall, the results in this section indicate that the coherent-array processor E_{COH} may not always be the best choice of multiple-array processor due to sensitivity to relative phase errors. In the presence of such errors, the processor E_{RelAmp} may provide an alternative choice. In none of the cases examined does the incoherent-array processor E_{INC} yield the best performance.

IV. APPLICATION TO DATA

A. SWellEx-96 data and processing

The data set is from the shallow water evaluation cell experiment 1996 (SWellEx-96) Event S5.[30] The data set contains multiple acoustic arrays, with demonstrated applications of MFP to a VLA,[5,8,9] a tilted VLA,[5,8] and a HLA[5,7] separately. The data set has also been analyzed in detail by others.[31,32] The SWellEx-96 data set was collected in May 1996 in shallow water of approximately 200 m depth. Two HLAs (S and N) were deployed on the seabed approximately 3 km apart. Each array had 32 elements with apertures of 255 m (S) and 240 m (N) at water depths of 198 m (S) and 213 m (N). Subsets of 27 elements (S and N) were used in the processing. The arrays were oriented with their line of bearing (LOB) −43° (S) and 34.5° (N) re clockwise north. For each array, element localization yielded accurate relative element positions within each array: element spacing was between 3.3 and 43.3 m and the arrays have a slight bow.[30] There has been no previous attempt to localize the relative positions of the two arrays. Array calibration data were available (per-array) and the two arrays were recorded on the same recording system.

Two multi-tone acoustic sources were towed along a track (Event S5) traversing between the two arrays (Fig. 4). Each source transmitted nine high-level (pilot) tones within 109–388 Hz, and the deeper source also transmitted a number of lower-level tones. The tow speed was 5 knots with source depths 54 and 9 m, respectively. Only the high-level tones from the deep source are considered here.

A model environment is built from previous work with this dataset: a measured sound speed profile in the water column [collected on 11 May 00:05:00 UTC],[30] array element location, and array position information as provided on the

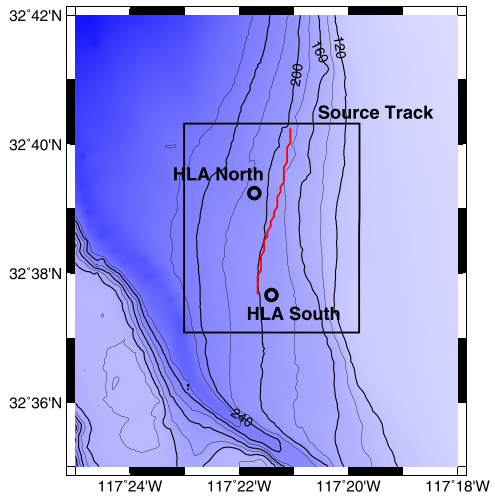

FIG. 4. (Color online) Part of the SWellEx-96 S5 event showing the path of the surface ship R/V Sproul. The ship towed a deep source at 54 m depth along roughly a 200 m isobath during the 34 min HLA recording. The black box indicates the search area used in MFP.

dataset website,[30] and a fluid seabed model[4,9,14,33] consisting of two sediment layers with gradient sound-speeds [constant density and attenuation] over a homogeneous half-space. Table II lists the seabed model parameters and their values [from Fig. 18 of Ref. 14].

Data, sampled at 3276.8 Hz, was transformed to the frequency domain with 8192-point fast Fourier transforms (2.5 s snapshot length, Hamming windowed), yielding frequency bin widths of 0.4 Hz. Data SCMs [Eqs. (11) and (A5)] were for each array formed from averages over 11 snapshots with 50% overlap, for segments of duration 15 s. A subset of data collected between 10 May 23:41:00 UTC and 11 May 00:15:30 UTC was processed. Midway into the tow, LFM sequences were transmitted briefly. The corresponding time segments (segment numbers 45–50, 118–121, and 128–132) were omitted from analysis. A total of 123 segments out of 138 segments were processed.

Processing frequencies were selected with a simple frequency tracker: from five frequency bins centered on each of the nominal source frequencies, the bin with maximum power (largest SCM eigenvalue) across the array is selected.

TABLE II. Seabed geoacoustic model parameters for the SWellEx-96 environment.

Parameter and units	Value	Description
h_1 (m)	30.0	Sediment layer 1 thickness
h_2 (m)	800.0	Sediment layer 2 thickness
c_{1T} (m/s)	1572	Sound speed—top of sediment layer 1
c_{1B} (m/s)	1593	Sound speed—bottom of sediment layer 1
c_{2T} (m/s)	1881	Sound speed—top of sediment layer 2
c_{2B} (m/s)	3246	Sound speed—bottom of sediment layer 2
c_3 (m/s)	5200	Sound speed—halfspace
ρ_1 (g/cm^3)	1.76	Density—sediment layer 1
ρ_2 (g/cm^3)	2.06	Density—sediment layer 2
ρ_3 (g/cm^3)	2.66	Density—halfspace
α_1 (dB/m-kHz)	0.20	Attenuation—sediment layer 1
α_2 (dB/m-kHz)	0.06	Attenuation—sediment layer 2
α_3 (dB/m-kHz)	0.02	Attenuation—halfspace

For individual arrays and with the incoherent-array processor, the tracker was applied to data from each array separately. Note that this may yield a small difference in data vector frequencies at each array due to differences in Doppler shift between the source and each array. The maximum Doppler shift is estimated to be $\pm 2.5/1500 = \pm 1.7 \times 10^{-3}$ times the source frequency (corresponding to ± 0.18 to ± 0.65 Hz for the pilot tones). For the other multiple-array processors, an alternative approach to selecting a common processing frequency from the bin with maximum power across both arrays also was tested. We found that the first approach gave the best results.

The 3D search volume for source positions is over (5, 6) km in (longitude, latitude) (50 m spacing) and 4–96 m in depth (2 m spacing), see Fig. 4. The replica fields were computed with the acoustic propagation model ORCA with the complex-valued mode search.[34] The water depth at the given array (S or N) was used in the respective replica field computations. Replica fields were computed at the selected processing frequencies of each array. Waveguide Doppler correction[35,36] was applied in the computation of replica fields. The procedure adopted here is for a moving source and fixed receivers:

(1) Compute horizontal wavenumbers $k_{rn}(\omega_r)$ and group speeds $u_{rn}(\omega_r)$ at the processing frequencies ω_r (where n is the mode index);
(2) Correct the horizontal wavenumbers to: $k'_{rn}(\omega_r) = k_{rn}/(1 + v_S/u_{rn})$ where v_S is the source radial velocity component (computed to each HLA element);
(3) compute replica fields at the processing frequency [with mode functions computed at the processing frequencies], using the corrected horizontal wavenumbers.

An explicit source spectrum correction[36] is here neglected. This would be required for frequency-coherent processing. Note that the waveguide Doppler correction ensures partial adjustment to a common source frequency in the ML-source terms.

The relative positions of the arrays were estimated using data at nine frequencies (pilot tones within 112–388 Hz) from time segments 41–44, 57–60, and 77–80. Data from the arrays were processed separately [with Eq. (13) for $J = 1$] with dense search volumes [5 m spacing in (longitude, latitude) and 1 m spacing in depth] centered around the true source positions. Minimizing the difference in source position estimates from the two arrays over the 12 segments yielded a relative array separation of 2.775 km, used in the following.

B. Results

In this section, results from processing with the multiple-array processors E_{COH} Eq. (10), E_{INC} Eq. (13), and E_{RelAmp} Eq. (15) and the 27-element N and S arrays are demonstrated. A correct localization is defined when the source position estimate is within error tolerances of 0.5 km in range (± 16 m in depth). Results are presented from processing with 1, 3, 5, or 9 frequencies. The nine-frequency results are with 112, 130, 148, 166, 201, 235, 283, 338, and 388 Hz; the five-frequency results are with 112, 148, 201, 338, and

388 Hz, the three-frequency results are with 112, 201, and 388 Hz, and the single-frequency results are with 201 Hz.

Figures 5(a)–5(e) shows slices of 3D-ambiguity volumes from processing of data at five frequencies from the deep source of SWellEx-96 event S5 source position NE of the N array [time segment 100] with (a) the S array, (b) the N array, and two arrays processed with the multiple-array processors (c) E_{COH}, (d) E_{INC}, and (e) E_{RelAmp} using Eqs. (10), (13), and (15), respectively. The slices are taken at the depth of the minimum of the ambiguity volumes, the depth indicated in the lower left corner of each panel. The color scale is the processor values relative to the minimum-misfit value, with bright colors corresponding to low processor values (low misfit) and different dynamic color scales are applied in panels (a) and (b) and (c)–(e). The true source position is (2.8, 4.53) km, in each panel at the crossing point of the white dashed lines. From each array beams of low processor values are observed. The lowest processor value (at the center of a white circle) is located within one of these beams. With the S array [Fig. 5(a)] the minimum (source location estimate) is at position (2.8, 4.95) km, with the N array [Fig. 5(b)] the minimum is at (3.85, 5.55) km. With multiple arrays, the lowest processor value is located at the intersection of two beams (one from each array). The position estimates are (3.9, 5.6) km with E_{COH} [Fig. 5(c)], (3.85, 5.55) km with E_{INC} [Fig. 5(d)], and (2.8, 4.65) km with E_{RelAmp} [Fig. 5(e)]. The position and depth estimates with E_{RelAmp} are within error tolerances.

Figures 6(a)–6(e) shows geographic plots of correctly estimated source positions with: (a) the S array, (b) the N array, (c) E_{COH}, (d) E_{INC}, and (e) E_{RelAmp}. Only estimated positions within range and depth error tolerances are included in the plots. The true source positions are based on the GPS position of the source ship,[30] corrected for an assumed ship-to-source range of 60 m; the true source depth

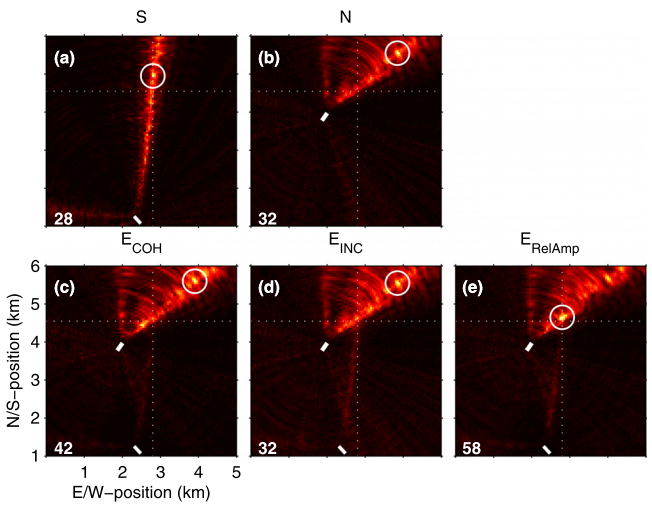

FIG. 5. (Color online) Horizontal slices of 3D-ambiguity volumes for SWellEx-96 S5 data at time segment 100 for (a) S array, (b) N array, and two arrays with multiple-array processors (c) E_{COH}, (d) E_{INC}, and (e) E_{RelAmp}. The white circle is centered at the position estimate, the true source position is at the crossing of the dashed white lines, and the white lines indicate arrays. The number (lower left) is the depth estimate and slice depth. Panels (a) and (b) are normalized independently from panels (c)–(e). The true source position is (2.8, 4.53) km and the true source depth is 54 m.

is assumed to be constant over the duration of the track. The solid black line indicates the true source track, and the array locations are indicated. The dotted blue lines indicate sectors within ±19° of the array endfire directions. These correspond to the endfire half-power beamwidth at the lowest processing frequency. With the S array, the source is well localized at the start of the track when it passes the array endfire at less than 1 km range, thereafter intermittently localized until the end of the track. With the N array, the source is localized for a few positions from the start of the track (at long range), and localized in passing the array broadside at closing range, while localization is again poor as the source approaches the array endfire sector. Poor localization here may be due to range error increasing due to water depth mismatch.[5] This also may explain the observed range offset at the start of the track. With the multiple-array processors, correct localizations are obtained over the entire track, also for positions where neither of the arrays individually localized the source. In particular, for positions between the two arrays and toward the end of the track. Visible gaps with no correct localizations coincide with the LFM transmission periods when no time segments were processed. Figures 6(f) and 6(g) show the true range and bearing (positive clockwise with respect to the array LOB) to the S and N arrays. The vertical axis is the time segment index along the track (15 s intervals from the south to the north ends of the track). These figures, when viewed with Figs. 6(c)–6(e), suggest that there is no apparent combination of source ranges or source bearings that yield consistently poor results, except for a period (time segments 50–55) when the source is approximately at equal range from both arrays and for a period (time segments 90–100) when the source is approximately at equal bearing to both arrays. Figures 6(h)–6(j) show the absolute range errors with the three multiple-array processors. Estimates with depth error within tolerance are indicated with closed symbols. The range errors are above tolerance (for all processors) for some segments near the end of the track (segments 111–117 and 122–126). In these segments, the source was not well localized with either of the arrays alone. With processor E_{INC} [Fig. 6(i)] there are intermittent time segments with range error above tolerance.

Figure 7 shows histograms of depth error (upper panels) and range error (lower panels) for the S and N arrays and for three multiple-array processors. For depth errors, negative values correspond to estimated depths shallower than true. Range error is the 2D distance and thus always positive. Each plot is based on 123 data points and is divided into bins of 8 m in depth and 0.25 km in range, respectively. In general, the depth error is widely distributed over the error intervals, though for the multiple-array processors with a peak centered on ±4 m depth error. The range error is widely distributed with single arrays, but peaked at low error (less than 0.5 km) with the multiple-array processors. Overall, depth localization is poor with the short HLAs used in this experiment, due to small effective vertical apertures hence poor depth resolution.[15]

Figure 8(a) shows the fraction of source position estimates within range error tolerance, FCL-position, with 1, 3, 5, and 9 frequencies included in the processing. The S array

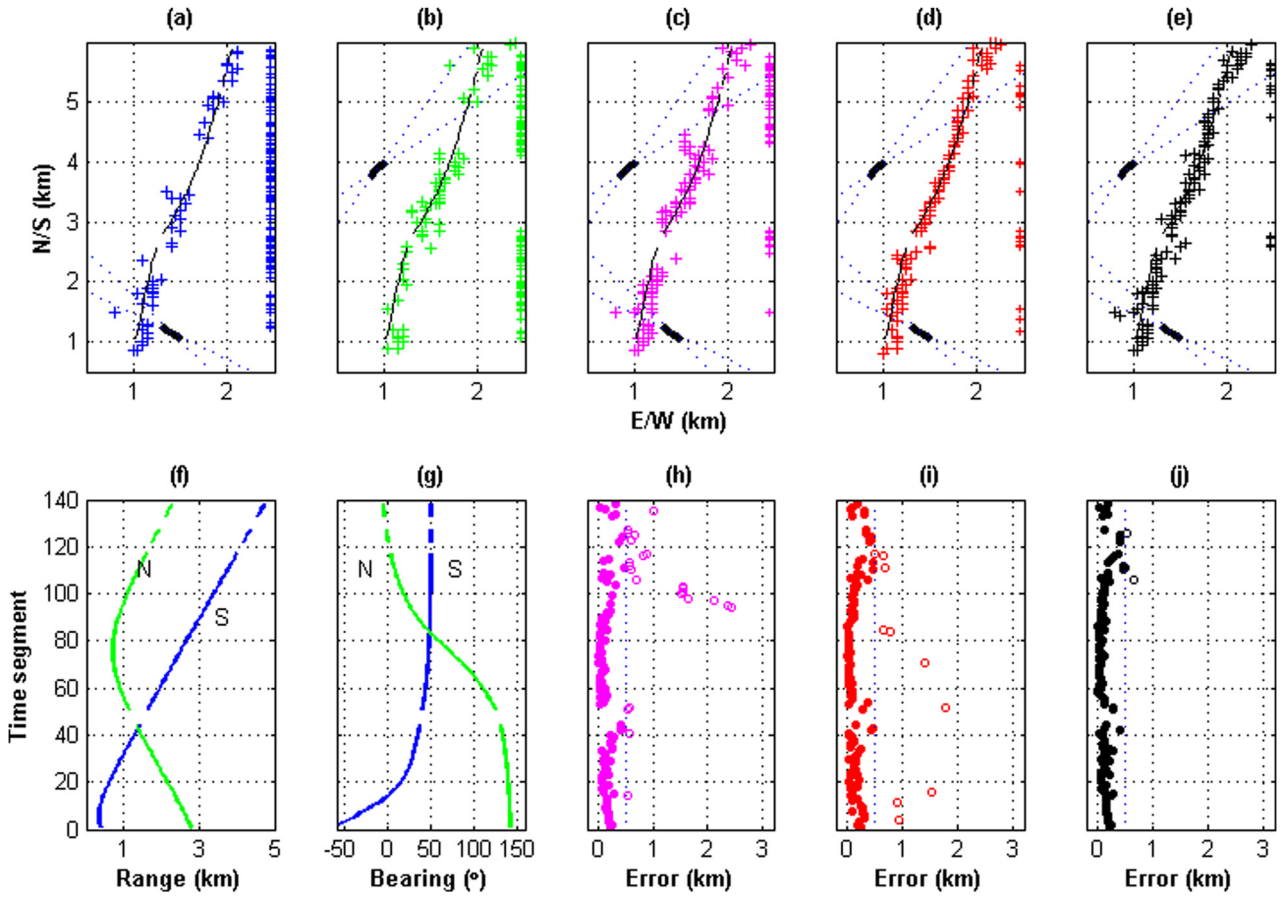

FIG. 6. (Color online) (a)–(e) Positions of correct localizations from data processed with (a) S array, (b) N array, and two arrays with multiple-array processors (c) E_{COH}, (d) E_{INC}, and (e) E_{RelAmp}. Arrays indicated with black symbols, dotted lines indicate sectors within ±19° of endfire, solid black line indicates source track (LFM segments omitted). Time segments not localized are indicated with small symbols to the right in each panel. (f) and (g) True range and bearing (positive clockwise re array LOB) to the S array and N array. (h)–(j) Range errors with processors (h) E_{COH}, (i) E_{INC}, and (j) E_{RelAmp}; filled symbols indicate depth error within tolerance (LFM segments omitted).

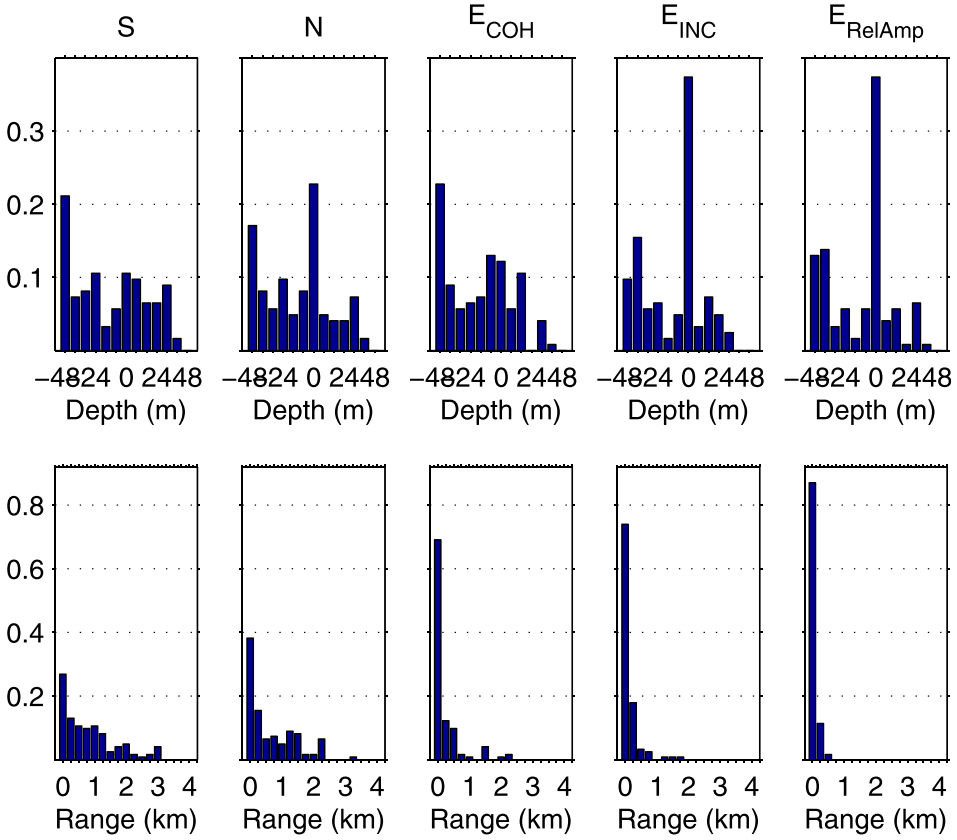

FIG. 7. (Color online) Normalized histograms of depth errors (upper panels) and positive range errors (lower panels). Horizontal panels are for different arrays and processors, indicated by text above each upper panel.

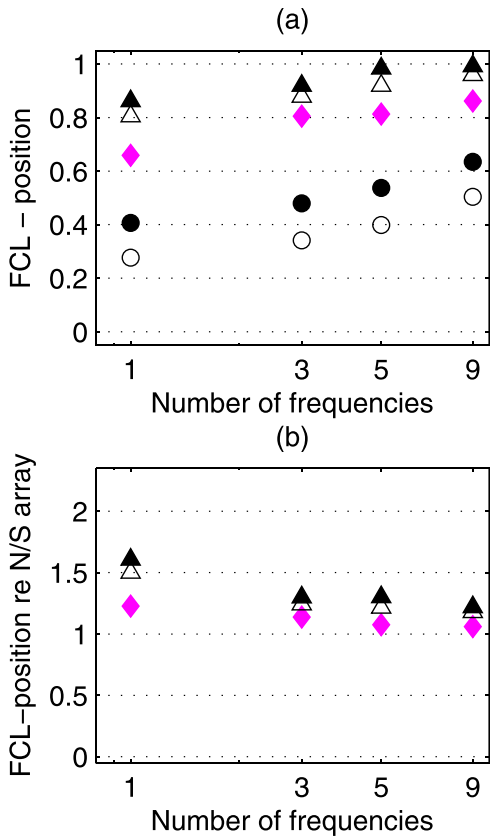

FIG. 8. (Color online) (a) Fraction of correct 2D-position localizations versus number of processed frequencies with S array (open circles), N array (circles), and two arrays with multiple-array processors E_{COH} (diamonds), E_{INC} (open triangles), and E_{RelAmp} (triangles). (b) Relative improvement in fraction of correct 2D-position localizations with the multiple-array processors over processing arrays individually.

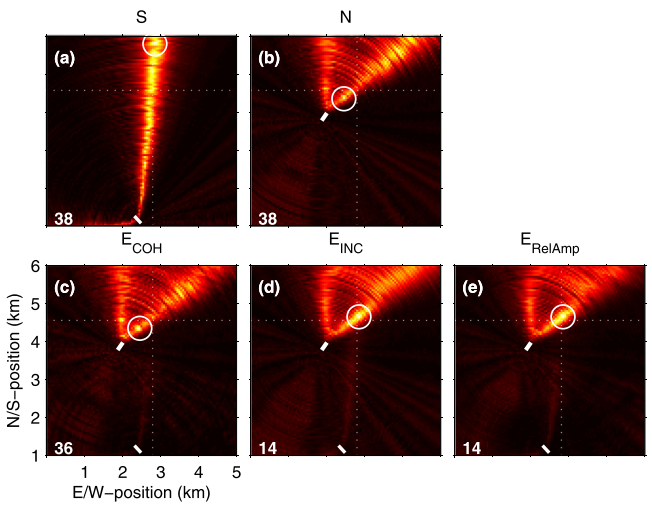

FIG. 9. (Color online) Horizontal slices of 3D-ambiguity volumes for SWellEx-96 S5 data at time segment 100 for (a) a 9-element array at S, (b) a 9-element array at N, and two 9-element arrays with multiple-array processors (c) E_{COH}, (d) E_{INC}, and (e) E_{RelAmp}. The white circle is centered at the position estimate, the true source position is at the crossing of the dashed white lines, and the white lines indicate arrays. The number (lower left) is the depth estimate and slice depth. Panels (a) and (b) are normalized independently from panels (c)–(e). The true source position is (2.8, 4.53) km and the true source depth is 54 m.

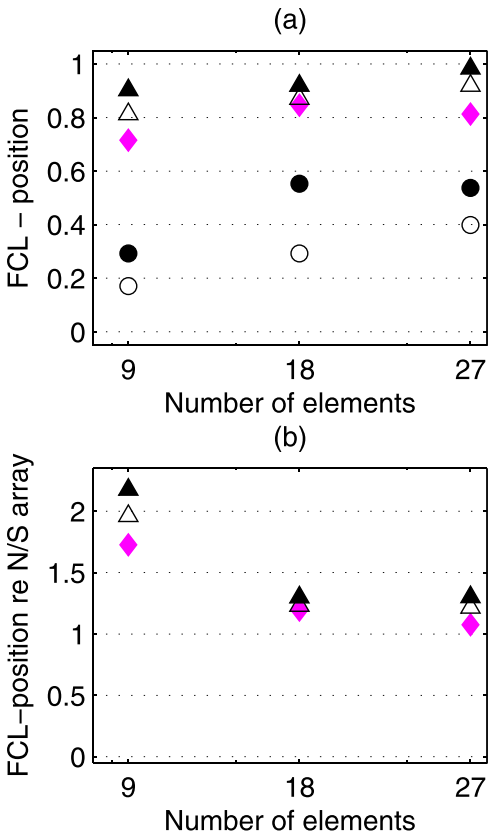

FIG. 10. (Color online) (a) Fraction of correct 2D-position localizations with 9-, 18-, and 27-element arrays and five frequencies processed with S array (open circles), N array (circles), and two arrays with multiple-array processors E_{COH} (diamonds), E_{INC} (open triangles), and E_{RelAmp} (triangles). (b) Relative improvement in fraction of correct 2D- position localizations with the multiple-array processors over processing arrays individually.

(open circles) and N array (circles) processed individually yield poorest results. The FCL-position increases from E_{COH} (diamonds) to E_{INC} (open triangles), with the best results obtained with E_{RelAmp} (triangles). For example, with five frequencies, the FCL-position is 0.40 with the S array, 0.53 with the N array, 0.81 with E_{COH}, 0.92 with E_{INC}, and 0.98 with E_{RelAmp}. Figure 8(b) shows the relative improvement in the FCL-position when processing with the multiple-array processors over the combined performance of the arrays processed individually. Correct localization with S or N arrays is here counted if the source is localized within range error tolerance with either the S or N array or both. With five frequencies, the relative improvement is 1.08 with E_{COH}, 1.21 with E_{INC}, and 1.30 with E_{RelAmp}. With one frequency, the relative improvement is 1.23 with E_{COH}, 1.5 with E_{INC}, and 1.61 with E_{RelAmp}. This demonstrates that considerable improvement in localization over processing arrays individually can be achieved with the multiple-array processors.

C. Short HLAs

To examine the performance of multiple-array processors with reduced data information, we consider the case of short arrays. For each of the S and N arrays, short arrays are formed by selecting the first 9 (or 18) elements thus forming arrays of length approximately 55 (or 163) m. (An

alternative, not examined here, would be to remove elements while retaining the full lengths of the arrays.) Figure 9 shows slices of 3D-ambiguity volumes from processing of data at five frequencies with (a) the 9-element S array, (b) the 9-element N array, and two 9-element arrays (S and N) processed with (c) E_{COH}, (d) E_{INC}, and (e) E_{RelAmp}, for source position NE of the N array [time segment 100]. In Figs. 9(a) and 9(b), the beams emanating from each array are broad and provide little range discrimination, and the position estimates are incorrect. With E_{INC} and E_{RelAmp} beams from each array intersect to produce a position estimate within the range error tolerance (the depth estimate is incorrect).

Figure 10(a) shows the fraction of source position estimates within range error tolerance, FCL-position, with five processing frequencies and varying number of array elements/lengths: 9 elements/55 m, 18 elements/163 m, and 27 elements/255 m. Processor E_{RelAmp} provides overall better results than E_{INC} and E_{COH}. Figure 10(b) shows the relative improvement in FCL-position when processing with the multiple-array processors over the combined performance of the arrays processed individually. With processor E_{RelAmp}, the relative improvement is 1.30 with 27-element arrays and with 18-element arrays, increasing to 2.18 with 9-element arrays.

V. SUMMARY AND DISCUSSION

This paper has developed ML matched-field processors for multiple-snapshot data and multiple arrays with varying assumptions on inter-array source spectral information. Three processors were derived for various assumptions on relative source spectral information (amplitude and phase at different frequencies) between arrays (and snapshot-to-snapshot). The processors implicitly apply weighting by estimated error variances. The processors were applied to towed-source data recorded at two horizontal arrays (of length 255 m) deployed on the seabed and approximately 3 km apart in shallow (200 m depth) water from the SWellEx-96 experiment.

A simulation with two HLAs in a range-independent shallow water environment showed that the coherent-array processor (E_{COH}) yielded the overall best localization performance in a perfectly known model environment. In the presence of relative (inter-array) phase error (e.g., a time synchronization error or random phase error) the performance of this processor can be degraded such that the coherent-array processor does not yield the best localization performance. The relative-amplitude processor (E_{RelAmp}), which assumes relative array calibrations known (can typically be assumed for arrays used with MFP), is robust to relative phase error and can provide an alternative to the coherent-array processor. The relative-amplitude processor yields improved performance over the incoherent-array processor (E_{INC}).

Results from processing of 123 time segments (about 31 min) from the deep source from Event S5 of the SWellEx-96 dataset yielded improved source localization results when processing multiple arrays over those obtained with single arrays. The coherent-array processor provided a much better localization performance than the best (N) array alone, and some improvement over the combined performance of the two arrays (S and N) processed individually. The coherent-array processor is sensitive to errors in time synchronization (this does not apply here as the arrays were cabled together) and array element localizations (for each array, all elements were carefully localized) and also is sensitive to phase errors due to relative array positions (the positions here estimated from the data) and other model mismatch. The incoherent-array processor provided better results than the coherent-array processor, and a further improvement over the combined performance of the two arrays. This processor does not assume (hence is insensitive to) error in relative (inter-array) phase. Best results with these HLA data were obtained with the relative-amplitude array processor that assumes relative array calibrations known but does not apply inter-array phase information. This processor provided the best localization results at all combinations of processing frequencies (from 1 to 9) examined within the 112–388 Hz frequency band. The relative-amplitude array processor provided a narrower distribution in range errors than the other processors (also, the depth distribution was slightly more peaked around low errors than with the other processors). With short arrays (9- and 18-element arrays of length 55 and 163 m) the relative-amplitude processor also provided overall best results. Improved matched-field source localization performance with increased spatial aperture is well established for single HLAs.[15,16] The results obtained here demonstrate that improved source localization performance can be achieved with multiple-array processors for spatially-separated short HLAs that individually yield poor performance.

The results in this paper were obtained with ML processors where uncertainties in source amplitude/phase[37] and environment model parameters[23] are not explicitly modeled with *a priori* probability density functions. Multiple-array processors might be studied in the context of such uncertainties, applied to array configurations that include VLAs, other kinds of sensor data such as vector sensors,[38] extended to matched-field source tracking,[31,39–42] and other approaches to MFP.[32]

ACKNOWLEDGMENTS

This work was sponsored by the Norwegian Defence Research Establishment (D.T.) and by the Office of Naval Research (P.G. and W.S.H.). D.T. wishes to thank the Scripps Institution of Oceanography for a Visiting Scholar invitation, and Professor Stan E. Dosso (University of Victoria, Canada) for valuable discussions on multiple-array processors.

APPENDIX

This Appendix provides formulations for three additional ML multiple-array processors that parallel those derived in Sec. II B. Specifically, in Sec. II B the source relative amplitude was assumed constant across snapshots (the source phase assumed unknown). In this appendix, both the source relative phase and amplitude are assumed unknown

across snapshots (i.e., complex amplitude unknown). This source model would fit well for a broadband random radiator (e.g., ship radiated noise).

1. Coherent

A coherent-array processor that assumes relative amplitude and phase unknown for each snapshot has source term $S_{fk} = A_{fk}e^{i\theta_{fk}}$ and ML amplitude and phase estimates

$$A_{fk} = \frac{|\mathbf{d}_f^H(\mathbf{x})\mathbf{d}_{fk}|}{\|\mathbf{d}_f(\mathbf{x})\|_2^2}, \quad e^{i\theta_{fk}} = \left[\frac{\mathbf{d}_f^{\mathrm{H}}(\mathbf{x})\mathbf{d}_{fk}}{\mathbf{d}_{fk}^{\mathrm{H}}\mathbf{d}_f(\mathbf{x})}\right]^{1/2}. \tag{A1}$$

The processor is denoted E_{COH}^{uu}

$$E_{\mathrm{COH}}^{uu} = KN\sum_{f=1}^{F}\log_e\left\{\mathrm{Tr}\{\mathbf{C}_f\} - \frac{\sum_{k=1}^{K}|\mathbf{d}_{fk}^{\mathrm{H}}\mathbf{d}_f(\mathbf{x})|^2}{K\|\mathbf{d}_f(\mathbf{x})\|_2^2}\right\}, \tag{A2}$$

where the data SCM $\mathbf{C}_f$ with trace $\mathrm{Tr}\{\mathbf{C}_f\}$ was defined in Eq. (11).

2. Incoherent

An incoherent-array processor that assumes amplitude and phase unknown for each snapshot (i.e., the source is unknown across arrays and snapshots) has source term $S_{fjk} = A_{fjk}e^{i\theta_{fjk}}$ and ML amplitude and phase estimates

$$A_{fjk} = \frac{|\mathbf{d}_{fj}^H(\mathbf{x})\mathbf{d}_{fjk}|}{\|\mathbf{d}_{fj}(\mathbf{x})\|_2^2}, \quad e^{i\theta_{fjk}} = \left[\frac{\mathbf{d}_{fj}^{\mathrm{H}}(\mathbf{x})\mathbf{d}_{fjk}}{\mathbf{d}_{fjk}^{\mathrm{H}}\mathbf{d}_{fj}(\mathbf{x})}\right]^{1/2}. \tag{A3}$$

The processor is denoted E_{INC}^{uu} and can be written

$$E_{\mathrm{INC}}^{uu} = KN\sum_{f=1}^{F}\log_e\left\{\mathrm{Tr}\{\mathbf{C}_f\} - \sum_{j=1}^{J}\frac{\mathbf{d}_{fj}^{\mathrm{H}}(\mathbf{x})\mathbf{C}_{fj}\mathbf{d}_{fj}(\mathbf{x})}{\|\mathbf{d}_{fj}(\mathbf{x})\|_2^2}\right\}, \tag{A4}$$

where

$$\mathbf{C}_{fj} = \frac{1}{K}\sum_{k=1}^{K}\mathbf{d}_{fjk}^{\mathrm{H}}\mathbf{d}_{fjk}, \tag{A5}$$

is the data SCM for array j. For single arrays (with $J = 1$), processor [Eq. (A4)] is equivalent to the frequency-incoherent Bartlett processor often applied in matched-field localization [e.g., Eq. (3.11) with Eq. (3.4) in Ref. 26; see also Refs. 4, 5, 8, 9, 11, and 14].

3. Relative amplitude

A relative-amplitude processor that assumes relative amplitude and phase unknown for each snapshot has source term $S_{fjk} = A_{fk}e^{i\theta_{fjk}}$ and ML amplitude and phase estimates

$$A_{fk} = \frac{\sum_{j=1}^{J}|\mathbf{d}_{fj}^H(\mathbf{x})\mathbf{d}_{fjk}|}{\|\mathbf{d}_f(\mathbf{x})\|_2^2}, \quad e^{i\theta_{fjk}} = \left[\frac{\mathbf{d}_{fj}^{\mathrm{H}}(\mathbf{x})\mathbf{d}_{fjk}}{\mathbf{d}_{fjk}^{\mathrm{H}}\mathbf{d}_{fj}(\mathbf{x})}\right]^{1/2}. \tag{A6}$$

The processor is denoted E_{RelAmp}^{uu}

$$E_{\mathrm{RelAmp}}^{uu} = KN\sum_{f=1}^{F}\log_e\left\{\mathrm{Tr}\{\mathbf{C}_f\} - \frac{\sum_{k=1}^{K}\left(\sum_{j=1}^{J}|\mathbf{d}_{fjk}^{\mathrm{H}}\mathbf{d}_{fj}(\mathbf{x})|\right)^2}{K\|\mathbf{d}_f(\mathbf{x})\|_2^2}\right\}. \tag{A7}$$

The ML multiple-array processors derived in Sec. II B and in the appendix are summarized in Table I.

[1]A. B. Baggeroer, W. A. Kuperman, and H. Schmidt, "Matched field processing: Source localization in correlated noise as an optimum parameter estimation problem," J. Acoust. Soc. Am. **83**, 571–587 (1988).
[2]J. Ozard, "Matched field processing in shallow water for range, depth, and bearing determination: Results of experiments and simulation," J. Acoust. Soc. Am. **86**, 744–753 (1989).
[3]D. P. Knobles and S. K. Mitchell, "Broadband localization by matched-fields in range and bearing in shallow water," J. Acoust. Soc. Am. **96**, 1813–1820 (1994).
[4]N. O. Booth, P. A. Baxley, J. A. Rice, P. W. Schey, W. S. Hodgkiss, G. L. D'Spain, and J. J. Murray, "Source localization with broad-band matched-field processing in shallow water," IEEE J. Oceanic Eng. **21**(4), 402–412 (1996).
[5]G. L. D'Spain, J. J. Murray, and W. S. Hodgkiss, "Mirages in shallow water matched field processing," J. Acoust. Soc. Am. **105**, 3245–3265 (1999).
[6]A. M. Thode, G. L. D'Spain, and W. A. Kuperman, "Matched-field processing, geoacoustic inversion, and source signature recovery of blue whale vocalizations," J. Acoust. Soc. Am. **107**, 1286–1300 (2000).
[7]A. T. Abawi and J. M. Stevenson, "Matched field processing and tracking with sparsely populated line arrays," in *Proceedings of the Fifth European Conference on Underwater Acoustics*, edited by M. F. Zakharia, P. Chevret, and P. Dubail, Lyon, France (2000).
[8]N. O. Booth, A. T. Abawi, P. W. Schey, and W. S. Hodgkiss, "Detectability of low-level broad-band signals using adaptive matched-field processing with vertical aperture arrays," IEEE J. Oceanic Eng. **25**, 296–313 (2000).
[9]P. Hursky, W. S. Hodgkiss, and W. A. Kuperman, "Matched field processing with data-derived modes," J. Acoust. Soc. Am. **109**, 1355–1366 (2001).
[10]L. M. Zurk, N. Lee, and J. Ward, "Source motion mitigation for adaptive matched field processing," J. Acoust. Soc. Am. **113**, 2719–2731 (2003).
[11]M. Nicholas, J. S. Perkins, G. J. Orris, L. T. Fialkowski, and G. Heard, "Environmental inversion and matched-field tracking with a surface ship and L-shaped receiver array," J. Acoust. Soc. Am. **116**, 2891–2901 (2004).
[12]T. B. Neilsen, "Localization of multiple acoustic sources in the shallow ocean," J. Acoust. Soc. Am. **118**, 2944–2953 (2005).
[13]C. Debever and W. A. Kuperman, "Robust matched-field processing using a coherent broadband white noise constraint processor," J. Acoust. Soc. Am. **122**, 1979–1986 (2007).
[14]P. A. Forero and P. A. Baxley, "Shallow-water sparsity-cognizant source-location mapping," J. Acoust. Soc. Am. **135**, 3483–3501 (2014).
[15]C. W. Bogart and T. C. Yang, "Source localization with horizontal arrays in shallow water: Spatial sampling and effective aperture," J. Acoust. Soc. Am. **96**, 1677–1686 (1994).
[16]S. L. Tantum and L. W. Nolte, "On array design for matched–field processing," J. Acoust. Soc. Am. **107**, 2101–2111 (2000).
[17]B. Nichols and K. G. Sabra, "Cross-coherent vector sensor processing for spatially distributed glider networks," J. Acoust. Soc. Am. **138**, EL329–EL335 (2015).
[18]S. H. Abadi, A. M. Thode, S. B. Blackwell, and D. R. Dowling, "Ranging bowhead whale calls in a shallow-water dispersive waveguide," J. Acoust. Soc. Am. **136**, 130–144 (2014).

[19]D. Mennitt and M. Johnson, "Multiple-array passive acoustic source localization in urban environments," J. Acoust. Soc. Am. **127**, 2932–2942 (2010).
[20]D. Tollefsen and S. E. Dosso, "Source localization with multiple hydrophone arrays via matched-field processing," IEEE J. Ocean. Eng. **PP**(99), 1–9 (2016). Available from https://doi.org/10.1109/JOE.2016.2615720. The relative-amplitude multiple-array processor was first presented in S. E. Dosso, "Matched-field source localization with non-synchronized sensor arrays," J. Acoust. Soc. Am. **135**, 2360 (2014).
[21]D. R. Del Balzo, C. Feuillade, and M. R. Rowe, "Effects of water-depth mismatch on matched-field localization in shallow water," J. Acoust. Soc. Am. **83**, 2180–2185 (1988).
[22]A. M. Richardson and L. W. Nolte, "*A posteriori* source localization in an uncertain sound speed, deep ocean environment," J. Acoust. Soc. Am. **89**, 2280–2284 (1991).
[23]S. E. Dosso and M. J. Wilmut, "Bayesian focalization: Quantifying source localization with environmental uncertainty," J. Acoust. Soc. Am. **121**, 2567–2574 (2007).
[24]Y. Le Gall, S. E. Dosso, F.-X. Socheleau, and J. Bonnel, "Bayesian source localization with uncertain Green's function in an uncertain shallow water ocean," J. Acoust. Soc. Am. **139**, 993–1004 (2016).
[25]W. Xu, A. B. Baggeroer, and H. Schmidt, "Performance analysis for matched-field source localization: Simulations and experimental results," IEEE J. Ocean. Eng. **31**, 325–344 (2006).
[26]C. F. Mecklenbräuker and P. Gerstoft, "Objective functions for ocean acoustic inversion derived by likelihood methods," J. Comp. Acoust. **8**, 259–270 (2000).
[27]C.-F. Huang, P. Gerstoft, and W. S. Hodgkiss, "Uncertainty analysis in matched-field geoacoustic inversions," J. Acoust. Soc. Am. **119**, 197–207 (2006).
[28]S. E. Dosso and M. J. Wilmut, "Estimating data uncertainty in matched-field geoacoustic inversion," IEEE J. Ocean. Eng. **31**, 470–479 (2006).
[29]S. E. Dosso and M. J. Wilmut, "Maximum-likelihood and other processors for incoherent and coherent matched-field localization," J. Acoust. Soc. Am. **132**, 2273–2285 (2012).
[30]The SWellEx-96 Experiment, http://swellex96.ucsd.edu (Last viewed March 31, 2016).
[31]C. Yardim, P. Gerstoft, and W. S. Hodgkiss, "Geoacoustic and source tracking using particle filtering: Experimental results," J. Acoust. Soc. Am. **128**, 75–87 (2010).
[32]P. Gerstoft, A. Xenaki, and C. F. Mecklenbräuker, "Multiple and single snapshot compressive beamforming," J. Acoust. Soc. Am. **138**, 2003–2015 (2015).
[33]P. A. Baxley, N. O. Booth, and W. S. Hodgkiss, "Matched-field replica model optimization and bottom property inversion in shallow water," J. Acoust. Soc. Am. **107**, 1301–1323 (2000).
[34]E. K. Westwood, C. T. Tindle, and N. R. Chapman, "A normal mode model for acousto-elastic ocean environments," J. Acoust. Soc. Am. **100**, 3631–3645 (1996).
[35]C. A. Zala and J. M. Ozard, "Matched-field processing for a moving source," J. Acoust. Soc. Am. **92**, 403–417 (1992).
[36]B. A. Tan, P. Gerstoft, C. Yardim, and W. S. Hodgkiss, "Broadband synthetic aperture geoacoustic inversion," J. Acoust. Soc. Am. **134**, 312–322 (2013).
[37]Z.-H. Michalopoulou, "The effect of source amplitude and phase in matched field source localization," J. Acoust. Soc. Am. **119**, EL21–EL26 (2006).
[38]G. L. D'Spain, J. C. Luby, G. R. Wilson, and R. A. Gramann, "Vector sensors and vector sensor line arrays: Comments on optimal array gain and detection," J. Acoust. Soc. Am. **120**, 171–184 (2006).
[39]S. L. Tantum and L. W. Nolte, "Tracking and localization a moving source in an uncertain shallow water environment," J. Acoust. Soc. Am. **103**, 362–373 (1998).
[40]S. E. Dosso and M. J. Wilmut, "Comparison of focalization and marginalization in Bayesian tracking in an uncertain environment," J. Acoust. Soc. Am. **125**, 717–722 (2009).
[41]D. Tollefsen and S. E. Dosso, "Three-dimensional source tracking in an uncertain environment," J. Acoust. Soc. Am. **125**, 2909–2917 (2009).
[42]C. Yardim, Z.-H. Michalopoulou, and P. Gerstoft, "An overview of sequential Bayesian filtering in ocean acoustics," IEEE J. Ocean. Eng. **36**, 71–89 (2011).